LAWRENCE
LIVERMORE
NATIONAL
LABORATORY

LLNL-CONF-698027

Non-LTE Modeling of Radiatively Driven Dense Plasmas

H. A. Scott

July 18, 2016

19th International Conference on Atomic Processes in Plasmas
Paris, France
April 4, 2016 through April 8, 2016

Disclaimer

This document was prepared as an account of work sponsored by an agency of the United States government. Neither the United States government nor Lawrence Livermore National Security, LLC, nor any of their employees makes any warranty, expressed or implied, or assumes any legal liability or responsibility for the accuracy, completeness, or usefulness of any information, apparatus, product, or process disclosed, or represents that its use would not infringe privately owned rights. Reference herein to any specific commercial product, process, or service by trade name, trademark, manufacturer, or otherwise does not necessarily constitute or imply its endorsement, recommendation, or favoring by the United States government or Lawrence Livermore National Security, LLC. The views and opinions of authors expressed herein do not necessarily state or reflect those of the United States government or Lawrence Livermore National Security, LLC, and shall not be used for advertising or product endorsement purposes.

Non-LTE Modeling of Radiatively Driven Dense Plasmas

H.A. Scott

Lawrence Livermore National Laboratory. PO Box 808, Livermore, CA 94550, USA

hascott@llnl.gov

Abstract. There are now several experimental facilities that use strong X-ray fields to produce plasmas with densities ranging from ~1 to ~10^3 g/cm^3. Large laser facilities, such as the National Ignition Facility (NIF) and the Omega laser reach high densities with radiatively driven compression, short-pulse lasers such as XFELs produce solid density plasmas on very short timescales, and the Orion laser facility combines these methods. Despite the high densities, these plasmas can be very far from LTE, due to large radiation fields and/or short timescales, and simulations mostly use collisional-radiative (CR) modeling which has been adapted to handle these conditions. These dense plasmas present challenges to CR modeling. Ionization potential depression (IPD) has received much attention recently as researchers work to understand experimental results from LCLS and Orion [1,2]. However, incorporating IPD into a CR model is only one challenge presented by these conditions. Electron degeneracy and the extent of the state space can also play important roles in the plasma energetics and radiative properties, with effects evident in recent observations [3,4]. We discuss the computational issues associated with these phenomena and methods for handling them.

INTRODUCTION

Multiple experimental facilities can now produce plasmas with densities greater than solid density, up to nearly 10^3 g/cm^3. Large lasers achieve this by compressing material on ns timescales with shocks and ablation pressure. Targets used in experiments on the NIF and Omega lasers routinely reach these large densities at temperatures up to several keV, although conditions are not uniform and density and temperatures may vary by several decades across the compressed target. Even at these densities, the high temperatures and large radiation fields ensure that any elements in these plasmas that are not completely stripped remain out of LTE. Short-pulse lasers ionize and heat material on sub-ps timescales, too short for hydrodynamic expansion to occur. Again, because of the strong ionizing fields and short timescales, these plasmas also can remain far from LTE.

The main simulation tool for these non-LTE plasmas remains the collisional-radiative (CR) model, originally developed for simulating low-density plasmas [5]. Applying a CR model to these dense radiatively driven plasmas requires extensions to handle a variety of physical phenomena. At high densities, ionization potential depression and electron degeneracy become important, and excited state distributions expand to cover an increasingly large portion of state space, i.e. the enumeration of atomic states. Interactions with strong X-ray radiation also enlarge the accessible state space by driving transitions that would otherwise be negligible. In addition, either local coupling of narrow-band radiation from an XFEL or non-local coupling of transported radiation demands careful attention to line profiles and energy balance.

Each of these phenomena requires generalization of some aspect of the CR model, introducing additional complexity and computational cost. Here we consider some of the issues that arise, discuss methods for handling them, and present examples demonstrating the importance of including these phenomena in simulations.

CONTINUUM LOWERING

The starting point for almost all CR models is the development of an atomic model for each element, providing both the energy level structure for that element and information needed to calculate transition rates (e.g. oscillator strengths). This data is commonly provided for an "isolated atom", i.e. calculated in the absence of boundaries or neighboring ions. However, the plasma environment affects both the structure and the rates, and these changes must then be incorporated in the evaluation of the CR model rather than in the atomic data. At low densities, the changes are minor and can be incorporated easily. At high densities, the changes are dramatic and impact many aspects of the CR model.

In the "isolated atom" limit of vanishing density, the partition function for a given element (or charge state) becomes infinite, since the atomic levels extend to infinity in principal quantum number with increasing degeneracy but finite energy. The electrostatic potential due to the presence of free electrons and neighboring ions at a finite density effectively lowers the ionization potential and truncates the partition functions. This phenomenon is referred to as "pressure ionization", "continuum lowering" or "ionization potential depression" (IPD). At low densities, this truncation may happen at higher principal quantum number n than those included in the CR atomic data and the effects are (hopefully) negligible. Under conditions obtained in recent experiments [1,2], the truncation occurs in the neighborhood of $n \sim 2\text{-}3$. Theoretical modeling of these experimental results is currently an active research area, as extant IPD models are not completely satisfactory for these conditions.

A widely used model for IPD, due to Stewart and Pyatt [6], is reproduced here. An ion of net charge z after ionization experiences a reduction in ionization potential of magnitude

$$\Delta E_z = \left[\left(1+ a/\lambda_D\right)^{2/3} - 1\right] \Big/ 2\left(z^* + 1\right), \quad z^* = \sum_i z_i^2 N_i \Big/ \sum_i z_i N_i \tag{1}$$

where z_i is the ion charge, λ_D is the Debye radius and a is the ion sphere radius

$$\lambda_D = \left[\frac{4\pi e^2}{kT}(z^* + 1) n_e\right]^{-1/2}, \quad a = \left(\frac{3z}{4\pi n_e}\right)^{1/3} \tag{2}$$

and, for simplicity, we have assumed $T = T_e = T_i$. At low density / high temperature, this expression limits to the Debye-Hückel model, while at high density / low temperature, it limits to the ion sphere model

$$\frac{a}{\lambda_D} << 1: \ \Delta E_z = \frac{ze^2}{\lambda_D kT} \quad , \quad \frac{a}{\lambda_D} >> 1: \ \Delta E_z = \frac{3}{2}\frac{ze^2}{akT} \tag{3}$$

A straightforward implementation of this in a CR model simply deletes levels in each charge state z that are bound by less than ΔE_z. In practice, several difficulties arise from this simple implementation. The IPD changes the ionization balance by an amount depending on the plasma conditions, so the iterative process of obtaining a self-consistent value for n_e to maintain charge neutrality becomes more complicated. Since the existence of a particular bound state depends discontinuously on n_e, the iterations may oscillate rather than converge. Similar statements apply to constructing derivatives with respect to temperature and electron density, as the energy levels E_i now also depend on the plasma conditions. The derivatives themselves will also be discontinuous, possibly leading to numerical difficulties.

We also note that at high enough densities (or low enough temperatures), some charge states may end up with no bound states remaining, with the most neutral charge states disappearing first. Due to the approximate nature of the model, the remaining charge states may not be contiguous under all conditions. This can also lead to erroneous behavior in the CR model if not guarded against. The disappearance of the most neutral charge states at high density and low temperature crudely mimics the formation of nonlocalized conduction bands in metals, but a CR model lacks the necessary physics to transition to a solid state. See [7] for an attempt to link to some aspects of a solid state model.

Allowing the bound states to gradually disappear can ameliorate the problems associated with discontinuous behavior. Physical justifications for this are the broadening of the level with increased perturbations and fluctuations in the electrostatic potential due to thermal motions of the ions. In practice, the gradual disappearance is achieved by decreasing the degeneracy g_i of level i so that it smoothly vanishes over an appropriate range of densities. Zimmerman and More [8] introduced a simple version of this in the context of an average-atom model. A more comprehensive approach, the occupation probability formalism [9], derives the reduced degeneracies and partition function truncation from contributions of 2-particle interactions to the Helmholtz free energy, ensuring a thermodynamically consistent EOS in LTE. The application of this formalism to non-LTE simulations is discussed in [10].

An example of these effects under conditions less extreme than those of those of [1,2] is given in Figure 1, which shows the emissivity for a small amount of Ar (0.1% by number) doped into hydrogen at electron (ion) temperatures of 5 (10) keV, and mass densities of 0.25, 0.5 and 1.0 g/cc, corresponding to conditions of interest for experiments on Omega and NIF. The spectral region shown extends from just below the Lyman beta line to just above the ionization edge of H-like Ar. The dashed line in each of the three sets of spectra was calculated without any IPD, as evidenced by the constant position of the ionization edge. The spectra given by the blue lines include IPD (via the Stewart-Pyatt model) without degeneracy lowering (DL). The IPD lowers the ionization edge by an amount increasing with density and modifies the ionization balance slightly, leading to a slight increase in continuum emission, but does not affect the Lyman line emission. The spectra given by the red lines incorporate degeneracy lowering through a model that identifies the ionized fraction by integrating over the microfield distribution, resulting in decreased and broadened emission from the upper excited states.

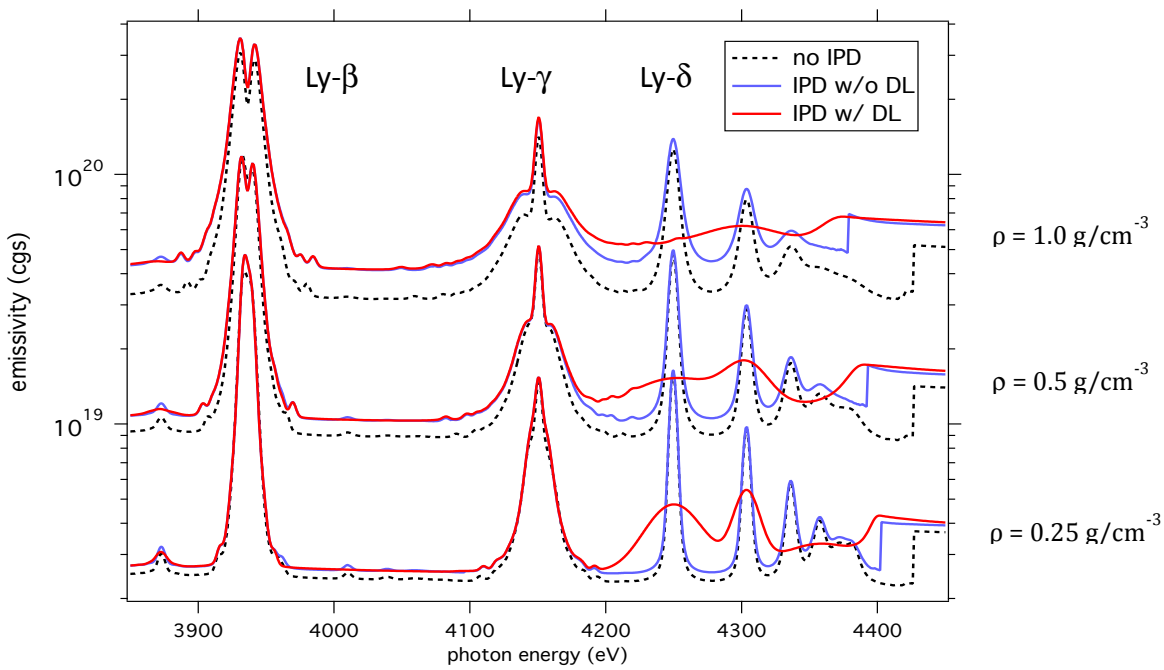

FIGURE 1. Spectral emissivity of an Ar-doped (0.1%) hydrogen plasma with T_e = 5 keV, T_i = 10 keV, and three different number densities, calculated without IPD (dashed line), with IPD but without degeneracy lowering (blue line), and with IPD including degeneracy lowering (red line).

ELECTRON DEGENERACY

Electron degeneracy has long been a concern in ICF and astrophysics, primarily because of its effects on dense matter equation of state and energetics. The advent of experiments on XFELs and dense plasma spectroscopy in high-convergence NIF implosions has renewed attention on degeneracy effects in CR modeling. Accordingly, we describe modifications to the standard CR approach to incorporate degeneracy effects.

For thermal electrons described by temperature T_e, the usual Maxwell-Boltzmann distribution is only valid at densities low enough so the electrons are not degenerate. Higher densities require use of the Fermi-Dirac distribution, in which the mean occupation of a state of energy ε is given by

$$F_e(\varepsilon) = \frac{1}{1+e^{(\varepsilon-\mu)/kT_e}} \tag{4}$$

and the electron distribution function is

$$f_e(\varepsilon) = 4\pi\left(\frac{2m_e}{h^2}\right)^{3/2} \varepsilon^{1/2} F_e(\varepsilon) \tag{5}$$

Here, μ is the chemical potential, related to the electron density n_e through

$$n_e = \int_0^\infty d\varepsilon f_e(\varepsilon) = \frac{4}{\sqrt{\pi}}\left(\frac{2\pi m_e kT_e}{h^2}\right)^{3/2} I_{1/2}(\mu / kT_e) \tag{6}$$

where I_m is the Fermi-Dirac integral of order m and we have assumed non-relativistic electrons with $\varepsilon = \frac{1}{2}m\mathbf{v}^2$. In the low-density limit, $-\mu/kT_e >> 1$, the chemical potential and electron density are related through

$$e^{\mu/kT_e} = \frac{n_e}{2}\left(\frac{h^2}{2\pi m_e kT_e}\right)^{3/2} = \frac{1}{2} n_e \lambda_e^3 \tag{7}$$

where λ_e is the electron thermal wavelength. Note that the mean occupation is equal to ½ for electrons with energy equal to the chemical potential, which limits to the Fermi energy E_f at zero temperature. For non-zero temperatures, degeneracy effects will be significant for electron energies of order the Fermi energy

$$E_F = \frac{h^2}{2m_e}\left(3\pi^2 n_e\right)^{2/3} \tag{8}$$

Transition rates, radiative properties and material properties must all be modified from the formulas used for low-density plasmas. A discussion of the thermodynamics of a degenerate electron gas is available from most textbooks on statistical mechanics, e.g. [11]. A result of particular utility for CR models is the Saha equation for degenerate electrons [12]

$$\frac{N_{i+1}}{N_i} e^{\mu/kT_e} = \frac{Z_{i+1}(T_e)}{Z_i(T_e)} e^{-\Delta E/kT_e} \tag{9}$$

that can be used to provide detailed balance relationships valid at any electron density by simply substituting $e^{\mu/kT}$ for each occurrence of ½ $n_e\lambda_e^3$.

Including degeneracy effects, the transition rate for a collisional excitation of energy ΔE becomes

$$C_{ij}^{cx} = \int_{\Delta E}^{\infty} \mathrm{v}(\varepsilon)\sigma_c^{ij}(\varepsilon) f_e(\varepsilon)\left[1 - F_e(\varepsilon - \Delta E)\right] d\varepsilon \tag{10}$$

where the integral over the electron distribution now includes a blocking factor $\left[1 - F_e\right]$ for the outgoing electron of energy ε-ΔE. Expressing the cross section in terms of the collision strength $\Omega \propto \varepsilon\sigma$ (or equivalently, the Gaunt factor), the transition rate is proportional to the integral

$$I^{cx} = \frac{4}{\sqrt{\pi}} \frac{1}{\lambda_e^3} \int_{\Delta E}^{\infty} \Omega(\varepsilon) \frac{1}{1+e^{(\varepsilon-\mu)/kT_e}} \left[1 - \frac{1}{1+e^{(\varepsilon-\Delta E-\mu)/kT_e}}\right] \frac{d\varepsilon}{kT_e} \tag{11}$$

where we have omitted the constants relating Ω and εσ. Since the collision strength varies slowly with energy, we first assume that the collision strength is a constant. The integral can then be done analytically, giving

$$I^{cx} = \frac{4}{\sqrt{\pi}} \frac{\Omega}{\lambda_e^3} \frac{e^{-\Delta E/kT_e}}{1-e^{-\Delta E/kT_e}} \ln\left[\frac{1+e^{\mu/kT_e}}{1+e^{(\mu-\Delta E)/kT_e}}\right] \tag{12}$$

while the same integral in the absence of degeneracy gives

$$I_{nd}^{cx} = \frac{4}{\sqrt{\pi}} \frac{\Omega}{\lambda_e^3} e^{(\mu-\Delta E)/kT_e} \tag{13}$$

The ratio of these two integrals then provides a "degeneracy factor" which, when multiplied by a non-degenerate transition rate, produces the equivalent transition rate incorporating degeneracy effects

$$\beta^{cx} = \frac{e^{-\mu/kT_e}}{1-e^{-\Delta E/kT_e}} \ln\left[\frac{1+e^{\mu/kT_e}}{1+e^{(\mu-\Delta E)/kT_e}}\right] \tag{14}$$

The expression in brackets varies slowly with μ/kT_e, becoming a constant, $\Delta E/kT_e$, in the high-density limit. The transition rate does not increase further with electron density, unlike the non-degenerate case, being restricted by the limiting value of the electron distribution function.

While the collision strength is not strictly constant, small deviations do not affect the degeneracy factor significantly. For collision strengths well approximated by a constant plus a logarithmic term, the formula underestimates the numerical degeneracy factor by at most a factor of a few while the degeneracy factor itself decreases by ten orders of magnitude. Collision strengths of forbidden transitions tend to vary in leading order as ε^{-1} or ε^{-2} and for these transitions the formula overestimates the degeneracy factor by a similar factor. If higher accuracy is desired, numerical integrations corresponding to $\ln(\varepsilon)$ and ε^{-n} terms could provide slowly varying corrections to the above degeneracy factor.

A collisional ionization of energy ΔE produces two outgoing electrons of energy ε' and ε-ε'-ΔE and the transition rate integral contains blocking factors for both electrons

$$C_{ij}^{ci} = \int_{\Delta E}^{\infty} d\varepsilon\, \mathrm{v}(\varepsilon) f_e(\varepsilon) \int_0^{\Delta E} d\varepsilon' \sigma_c^{ij}(\varepsilon,\varepsilon')\left[1-F_e(\varepsilon')\right]\left[1-F_e(\varepsilon-\varepsilon'-\Delta E)\right] \tag{15}$$

Assuming that the differential cross section $\sigma(\varepsilon,\varepsilon')$ is independent of ε' and that the collision strength is independent of ε leads to a degeneracy factor for collisional ionization rates of

$$\beta^{ci} = e^{-(\mu-\Delta E)/kT_e} \int_{\Delta E}^{\infty} \frac{d\varepsilon}{1+e^{(\varepsilon-\mu)/kT_e}} \frac{1}{(\varepsilon-\Delta E)} \int_0^{\varepsilon-\Delta E} \frac{d\varepsilon'}{kT_e}\left[1-\frac{1}{1+e^{(\varepsilon-\varepsilon'-\mu)/kT_e}}\right]\left[1-\frac{1}{1+e^{(\varepsilon-\varepsilon'-\Delta E-\mu)/kT_e}}\right] \tag{16}$$

The double integral cannot be done analytically, but the expression

$$\beta^{ci} \approx \zeta\beta^{cx} \ , \ \zeta = \ln\left(1+e^{-\mu/kT_e}\right) \tag{17}$$

provides a very good approximation over a wide range of parameters.

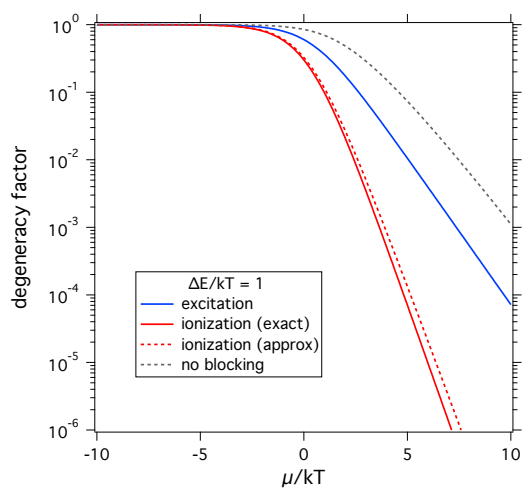

FIGURE 2. Degeneracy factors for a transition with $\Delta E/kT = 1$. The upper dashed line gives the degeneracy factor in the absence of blocking factors. The blue line gives the degeneracy factor for excitation β^{cx}. The solid red line gives the degeneracy factor for ionization β^{ci} from Eq. 17, while the solid red line gives β^{ci} from a numerical evaluation of Eq.16.

Figure 2 presents these degeneracy factors for a transition with $\Delta E/kT_e = 1$. Choosing a different value of $\Delta E/kT_e$ shifts the curves slightly in μ/kT_e, but does not change their character. The upper dashed line gives the degeneracy factor in the absence of blocking factors, showing the difference in collisional rates due to using a Fermi-Dirac distribution instead of a Maxwell-Boltzmann distribution for the electrons.

The degeneracy factor for ionization drops more sharply with increasing μ/kT_e than the factor for excitation, due to the presence of blocking factors for both outgoing electrons. The main approximation here is the assumption that the differential cross section is independent of the outgoing electron energy. However, numerical integrations using a more realistic differential cross section [13] give results that are virtually indistinguishable from those obtained with a differential cross section independent of ε'.

Electron degeneracy also affects other transitions that involve free electrons. Photoionization produces a single outgoing free electron and requires an appropriate blocking factor, decreasing the absorption coefficient for photons close to threshold energy. Autoionization transitions should be treated in a similar manner, although the emitted electrons tend to be of relatively high energy and minimally affected by degeneracy.

Transitions between free electron states, i.e. bremsstrahlung and inverse bremsstrahlung, do not affect the bound state distributions but can be critical in determining the energy balance of a dense radiating plasma. The effects of degeneracy on these absorption and emission processes have been discussed in the literature in varying levels of detail, e.g. [14,15], but can be understood in terms of the previous discussion. Each such (absorption) transition involves a single incoming electron of energy ε and a single outgoing electron of energy ε-$h\nu$, with a cross-section inversely proportional to electron velocity (incorporating various quantum effects into a Gaunt factor). Accordingly, under the assumption of a constant Gaunt factor, the degenerate and non-degenerate treatments differ by the factor β^{ex}, with the substitution of $h\nu$ for ΔE. We note that plasma collective effects can also strongly affect radiative properties [16] and assume that these effects can be treated independently of degeneracy effects.

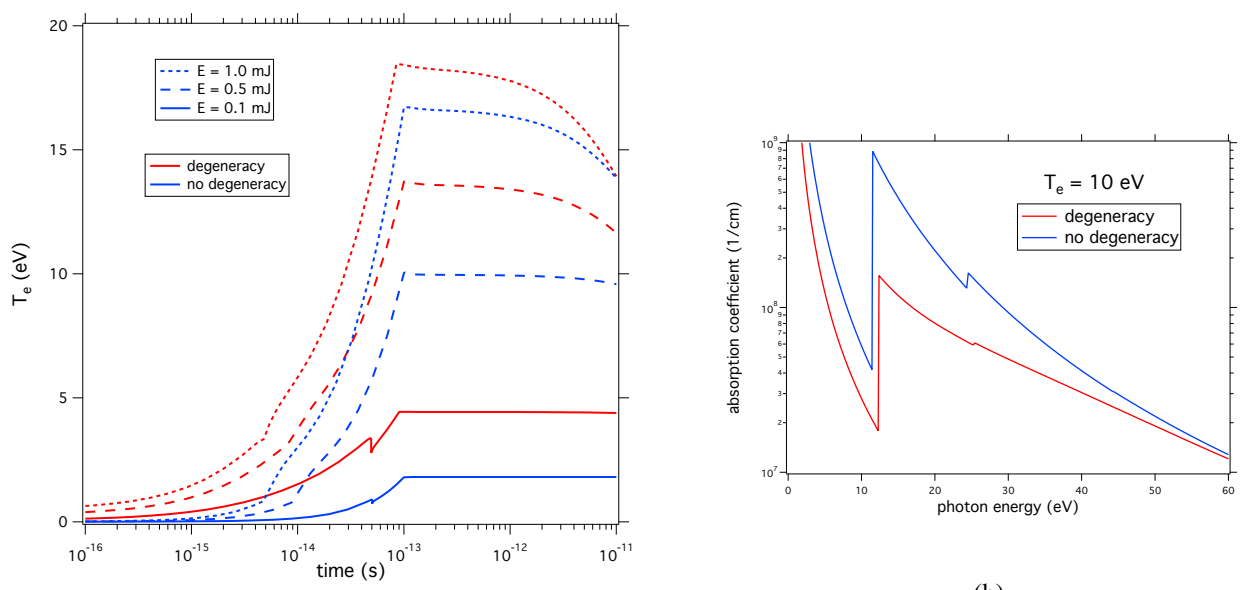

(a) (b)

FIGURE 3. (a) Time evolution of the electron temperature of the central zone of a 0.01 um thick foil of solid Fe irradiated with a 100 fs pulse of 8 keV X-rays and 10 µm diameter spot size. The three sets of curves correspond to different pulse energies: upper – 0.1 mJ, middle – 0.5 mJ, lower – 1.0 mJ. For each pairs of curves, the upper (red) curve includes the effects of degeneracy, while the lower (blue) curve does not include degeneracy. (b) Absorption coefficient for solid density Fe at $T_e = 10$ eV. The lower (red) curve includes the effects of degeneracy, while the upper (blue) curve does not include degeneracy. The Fermi energy of this material is ~40 eV.

Blocking factors for photoionizing transitions can be important for XFEL applications, despite the use of multi-keV photons. Fermi energies for solid materials vary from a few tens to a few hundred eV, directly affecting ionization and heating rates for experiments driven by photons slightly above ionization edges. For experiments that heat materials to tens or hundreds of eV, both heating and cooling will be significantly affected. An example of this

is given in Figure 3a, which displays the temperature evolution of the center of a 0.01 μm thick foil of solid Fe driven with a 100 fs square pulse of 8 keV X-rays, with three sets of curves corresponding to different beam energies. Although the absorption of the 8 keV photons is not affected by degeneracy, higher temperatures result from the decreased specific heat of the degenerate matter. Increased cooling after the drive pulse shuts off is due to reduced trapping of ~thermal emitted photons, also resulting in more uniform spatial profiles. Figure 3b shows the effect of degeneracy on the absorption coefficient of solid Fe at a temperature of 10 eV for photons of energy below 60 eV. The Fermi energy of the target material varied between 40 and 45 eV during the simulations.

STATE SPACE COVERAGE

The necessity to treat high densities also puts constraints on atomic models. As densities and collisional rates increase, excited states – including those containing multiple excited electrons – hold an increasingly larger fraction of state populations, making it important to include these states. This effect can be analyzed easily with the Saha-Boltzmann equation in the LTE limit. For radiatively-driven systems, the need to accommodate ionization and excitation by multi-keV photons also requires the inclusion of states with one or more holes in all attainable inner shells. Both these effects greatly increase the number of configurations required in the atomic models used in simulations.

Figure 4 demonstrates these effects for optically thin Fe plasma simulated with atomic models containing configurations up to a maximum principal quantum number 10. Figure 4a shows the fractional number of states that have at least one electron in the shell identified by principal quantum number n as a function of electron density for a fixed electron temperature of 200 eV. For all shells with n>3, the fractional number increases with electron density (approximately as n_e^2) until continuum lowering begins to destroy those states. Figure 4b shows the simulated emission spectrum from Fe at a temperature of 100 eV and electron density of 10^{24} cm^{-3} irradiated by 10 TW/cm^2 of 12 keV photons. The individual spectra were calculated with screened-hydrogenic atomic models that differed only in the maximum number of excited electrons allowed in the set of superconfigurations used to construct the model. The major spectral features differ considerably when calculated with 2 or 3 excitations, and do not converge until 5 or more excitations. The use of superconfigurations here does not produce a realistic spectrum for these conditions, but the distinct spectral features do facilitate an understanding of the effects of the state space on the emission.

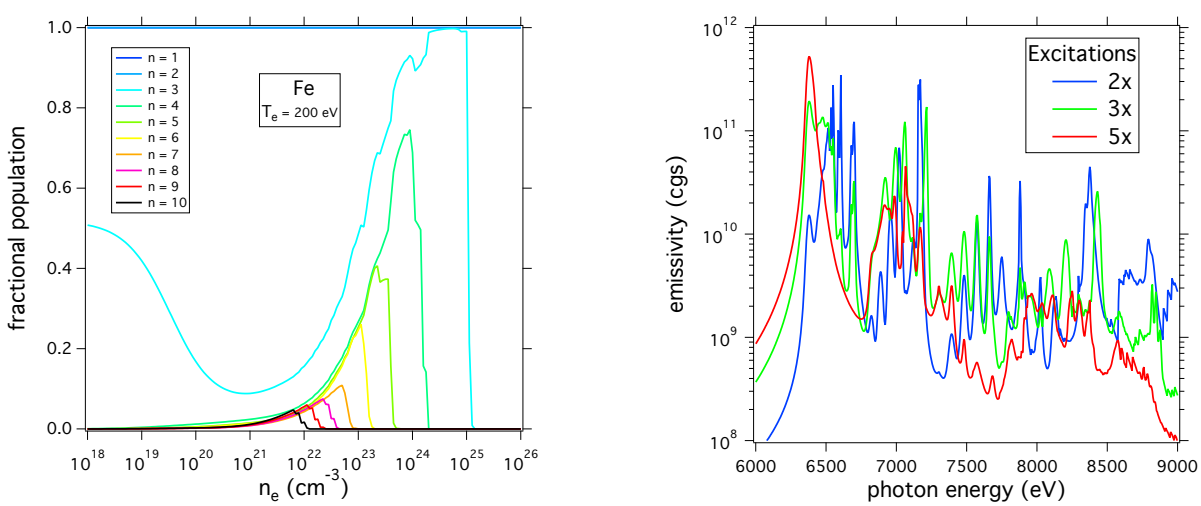

(a) (b)

FIGURE 4. (a) Fractional number of states populating shells with principal quantum numbers 1-10 for Fe at a temperature of T_e = 200 eV as a function of electron density. (b) Emissivity of Fe at a temperature of T_e = 100 eV and fixed electron density of n_e = 10^{24} cm^{-3} irradiated by 10 TW of 12 keV photons. The curves correspond to atomic models including superconfigurations with different maximum numbers of excited electrons – 2 (blue), 3 (green), 5 (red).

INTEGRATED SIMULATIONS

The preceding discussion has focused on three aspects of modeling dense, radiatively driven plasmas with CR models, with each aspect considered independently. Many experiments cover a wide range of densities and temperatures as they evolve in space and/or time and simulations must do likewise. Radiation can then spatially couple different regions with disparate conditions and effects from one region may influence the others.

As an example of this, we consider the spectrum obtained from an imploded NIF capsule presented and partially analyzed in [3]. A portion of the experimental spectrum is reproduced in Fig. 5a, with identifications for a few features due to Ge emission and absorption. The analysis in [3] considered only the emission feature between 10.0 and 10.5 keV, labeled as He-α but including significant emission from related transitions from Li-, Be-, B- and C-like Ge. Figure 5a also shows a simulated spectrum produced with a 1D model constructed by O. Ciricosta consisting of 4 uniform concentric shells. The shells correspond to features of the original target: (1) the (unablated) capsule shell, (2) DT ice, (3) DT gas with ablator material mixed in, and (4) DT gas. A pie diagram of the model is given in Fig. 5b, with each shell labeled with values of electron temperature and electron density used to produce the simulated spectrum.

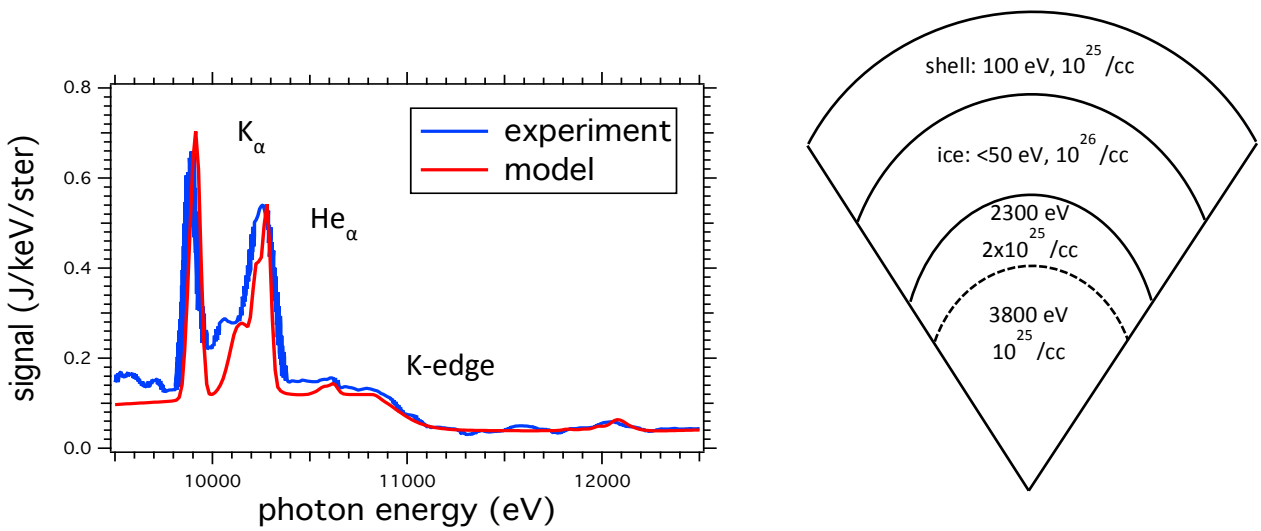

(a) (b)

FIGURE 5. (a) Experimental (blue) and modeled (red) spectra for the imploded NIF capsule discussed in [3], with identifications for a few major features due to Ge emission and absorption. (b) 4-region model constructed by O. Ciricosta for the imploded capsule. Each of the four regions is labeled with an estimated temperature and electron density. The shell is composed of CH doped with Ge, Si and Cu. The ice is composed of H. The remaining two regions comprise the hot spot, which is composed of H along with some shell material (without Cu).

The spectrum contains information on the conditions in each of the regions, with some features depending on conditions in multiple regions. The He-α emission is primarily dependent on the hot spot temperature and density, although producing the red wing of this feature requires more than a single temperature. The other strong features - K-α fluorescence, the position, shape and depth of the K-edge - are connected by radiation transport and depend upon dense plasma features.

As an example, Fig. 6a shows the spectra resulting from adjusting the temperature of the shell. The 1s-2p K-α feature, driven by radiation from the hot spot, depends on the ionization state of the shell, changing from strong fluorescence at low temperatures with minimal excitations, to absorption at temperatures high enough to ionize the material into the L-shell, providing 2p vacancies to enable absorptions to dominate. Producing this feature in a

simulation, in either absorption or emission, also requires that the state space for M-shell Ge accommodate the relevant transitions. The shape of the K-edge strongly reflects modification of the absorption edge by electron degeneracy; the shell conditions in the 4-shell model correspond to a Fermi energy of 350 eV. Similarly, changes in the IPD model will also affect the spectral features. The position of the K-edge depends on the amount of continuum lowering. The IPD model can also change the strength of the K-α feature and may also allow a K-β feature.

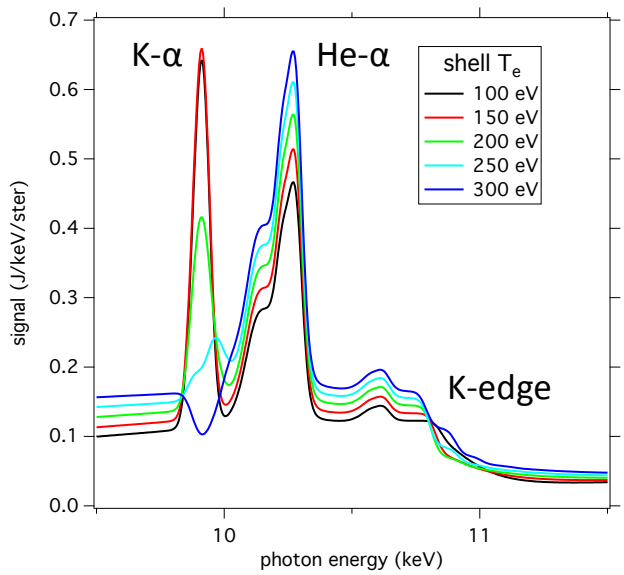

FIGURE 6. Spectra from a radiation transport / CR simulation of the capsule model for five different shell temperatures.

SUMMARY

Radiatively driven dense plasmas present challenges to CR modeling, requiring multiple extensions to the standard collisional-radiative formulation. Including electron degeneracy effects into rate calculations is relatively straightforward, particularly in an approximate formulation. Incorporating ionization potential depression is more problematic and a generally applicable model (with a comprehensive understanding of the phenomenon) is still lacking. An additional challenge is the need to identify the extensive range of state space and transitions that may be accessed during a simulation and to provide adequate coverage in the atomic data, a requirement made more pressing by the non-local coupling of material regions through radiation transport.

ACKNOWLEDGMENTS

We gratefully acknowledge fruitful conversations and collaborations with Felicie Albert, Bruce Hammel, Stefan Hau-Riege, Louisa Pickworth, and George Zimmerman of Lawrence Livermore National Laboratory, Sean Regan of the Laboratory for Laser Energetics, Stephanie Hansen of Sandia National Laboratories, and Orlando Ciricosta and Tom Preston of Oxford University.

This work performed under the auspices of U.S. Department of Energy by Lawrence Livermore National Laboratory under Contract DE-AC52-07NA27344.

REFERENCES

1. O. Ciricosta, S.M. Vinko, H.-K. Chung, *et al*, Phys. Rev. Lett. **109**, 065002 (2012).
2. D.J. Hoarty, P. Allan, S.F. James, *et al*, Phys. Rev. Lett. **110**, 265003 (2013).
3. S.P. Regan, R. Epstein, B.A. Hammel, *et al*, Phys. Rev. Lett. **111**, 045001 (2013).
4. L.A. Pickworth, B.A. Hammel, V.A. Smalyk, *et al*, Phys. Rev. Lett. **117**, 035001 (2016).
5. D.R. Bates, A.E. Kingston, R.W.P. McWhirter, Proc. R. Soc. **A267**, 297-312 (1962).
6. J.C. Stewart, K.D. Pyatt, Astrophys. J. **144**, 1203-1211 (1966).
7. B. Deschaud, O. Peyrusse, F.B. Rosmej, HEDP **15**, 22-29 (2015).
8. G.B. Zimmerman and R.M. More, JQSRT **23**, 517-522 (1980).
9. D.G. Hummer and D. Mihalas, Astrophys. J. **331**, 794-814 (1988).
10. I. Hubeny, D.G. Hummer and T. Lanz, Astron. Astrophys. **282**, 151-167 (1994).
11. R.K. Pathria, *Statistical Mechanics*, Pergamon Press, 1972.
12. H.C. Graboske, D.J. Harwood and F.J. Rogers, Phys. Rev. **186**, 210-225 (1969).
13. R.E.H. Clark, J. Abdallah, Jr., J.B. Mann, Astrophys J **381**, 597-600 (1991).
14. H. Totsuji, Phys. Rev. **A32**, 3005-3010 (1985).
15. S. Eliezer, P.T. Leon, J.M. Martinez-Val and D.V. Fisher, Laser and Particle Beams **21**, 599-607 (2003).
16. G. Bekefi, *Radiation Processes in Plasmas*, John Wiley & Sons, 1966.